Inorg. Chem. **2006**, *45*, 3990–3997

Structural and Spectroscopic Characterization of a Diruthenium *o*-Dioxolene Complex Possessing a Singly Occupied Molecular Orbital Delocalized over the Entire Molecule, $[Ru_2(3,6\text{-DTBDiox})_4]^-$

Katsunori Mochizuki,[†] Takashi Kawamura,[†] Ho-Chol Chang,[†,‡] and Susumu Kitagawa*[,†]

Department of Synthetic Chemistry and Biological Chemistry, Graduate School of Engineering, Kyoto University, Katsura, Nishikyo-ku, Kyoto 615-8510, Japan, and PRESTO, Japan Science and Technology Agency, 4-1-8 Honcho, Kawaguchi, Saitama 332-0012, Japan

Received December 23, 2005

Chemical oxidation of $[Ru_2^{6+}(3,6\text{-DTBCat})_4]^{2-}$ affords $[n\text{-}Bu_4N][Ru_2(3,6\text{-DTBDiox})_4]\cdot$acetone (**2**·acetone). The oxidized species was characterized by X-ray crystallographic analysis and EPR, and the delocalization of the unpaired electron over the entire molecule was indicated. This example showed that the utilization of redox-active ligands into a Ru_2 complex expanded the degree of freedom in the electronic structure. DFT calculations support this view, and the spin population was estimated to be approximately 18% and 82% for the Ru_2 core and the four dioxolene ligands, respectively.

Introduction

Diruthenium complexes with a direct Ru−Ru bond (Ru_2 complexes) have received considerable attention, and a number of Ru_2 complexes have been synthesized in the last half century.[1] One of the fascinating aspects of Ru_2 complexes is the variation in formal oxidation state of the Ru_2 core, and multi-redox activity of the Ru_2 core has been frequently reported.[2] In previous studies, several multinuclear Ru complexes equipped with heterometal dinuclear[3] or triruthenium cores,[4] extended Ru−Ru bonds in nanowires,[5] and assembled Ru_2 cores[6] have been synthesized in the development of functional materials with novel electron configurations.

On the other hand, the utilization of the redox-active ligand into a dinuclear complex is another approach to expand the degree of freedom in the electronic structure of a dinuclear complex. Several Ru_2 complexes with redox-active ligands such as porphyrin,[7] corrole,[8] and dioxolene (Diox)[9−12] have

* To whom correspondence should be addressed. E-mail: kitagawa@sbchem.kyoto-u.ac.jp. Tel: +81-75-383-2733. Fax: +81-75-383-2732.
† Kyoto University.
‡ Japan Science and Technology Agency.

(1) Angaridis, P. In *Multiple Bonds between Metal Atoms*, 3rd ed.; Cotton, F. A., Murillo, C. A., Walton, R. A., Eds.; Springer-Science and Business Media Inc.: New York, 2005; Chapter 9.
(2) (a) Ren, T. *Organometallics* **2005**, *24*, 4854. (b) Kadish, K. M.; Phan, T. D.; Wang, L. L.; Giribabu, L.; Thuriere, A.; Wellhoff, J.; Huang, S. R.; Van Caemelbecke, E.; Bear, J. L. *Inorg. Chem.* **2004**, *43*, 4825. (c) Shi, Y. H.; Yee, G. T.; Wang, G. B.; Ren, T. *J. Am. Chem. Soc.* **2004**, *126*, 10552. (d) Han, B. C.; Shao, J. G.; Ou, Z. P.; Phan, T. D.; Shen, J.; Bear, J. L.; Kadish, K. M. *Inorg. Chem.* **2004**, *43*, 7741. (e) Kadish, K. M.; Wang, L. L.; Thuriere, A.; Van Caemelbecke, E.; Bear, J. L. *Inorg. Chem.* **2003**, *42*, 834. (f) Miyasaka, H.; Izawa, T.; Sugiura, K.; Yamashita, M. *Inorg. Chem.* **2003**, *42*, 7683. (g) Bear, J. L.; Chen, W. Z.; Han, B. C.; Huang, S. R.; Wang, L. L.; Thuriere, A.; Van Caemelbecke, E.; Kadish, K. M.; Ren, T. *Inorg. Chem.* **2003**, *42*, 6230.
(3) (a) Collman, J. P.; Harford, S. T.; Maldivi, P.; Marchon, J. C. *J. Am. Chem. Soc.* **1998**, *120*, 7999. (b) Collman, J. P.; Harford, S. T.; Franzen, S.; Marchon, J. C.; Maldivi, P.; Shreve, A. P.; Woodruff, W. H. *Inorg. Chem.* **1999**, *38*, 2085. (c) Collman, J. P.; Harford, S. T.; Franzen, S.; Shreve, A. P.; Woodruff, W. H. *Inorg. Chem.* **1999**, *38*, 2093.
(4) (a) Sheu, J. T.; Lin, C. C.; Chao, I.; Wang, C. C.; Peng, S. M. *Chem. Commun.* **1996**, 315. (b) Kuo, C. K.; Chang, J. C.; Yeh, C. Y.; Lee, G. H.; Wang, C. C.; Peng, S. M. *J. Chem. Soc., Dalton Trans.* **2005**, 3696.
(5) (a) Masciocchi, N.; Moret, M.; Cairati, P.; Ragaini, F.; Sironi, A. *J. Chem. Soc., Dalton Trans.* **1993**, 471. (b) Masciocchi, N.; Sironi, A.; Chardon-Noblat, S.; Deronzier, A. *Organometallics* **2002**, *21*, 4009.
(6) (a) Shiu, K. B.; Lee, H. C.; Lee, G. H.; Wang, Y. *Organometallics* **2002**, *21*, 4013. (b) Angaridis, P.; Berry, J. F.; Cotton, F. A.; Murillo, C. A.; Wang, X. P. *J. Am. Chem. Soc.* **2003**, *125*, 10327. (c) Xu, G. L.; Zou, G.; Ni, Y. H.; DeRosa, M. C.; Crutchley, R. J.; Ren, T. *J. Am. Chem. Soc.* **2003**, *125*, 10057.
(7) (a) Collman, J. P.; Barnes, C. E.; Swepston, P. N.; Ibers, J. A. *J. Am. Chem. Soc.* **1984**, *106*, 3500. (b) Collman, J. P.; Arnold, H. J.; Fitzgerald, J. P.; Weissman, K. J. *J. Am. Chem. Soc.* **1993**, *115*, 9309. (c) Collman, J. P.; Harford, S. T. *Inorg. Chem.* **1998**, *37*, 4152.
(8) (a) Jérôme, F.; Billier, B.; Barbe, J. M.; Espinosa, E.; Dahaoui, S.; Lecomte, C.; Guilard, R. *Angew. Chem., Int. Ed.* **2000**, *39*, 4051. (b) Simkhovich, L.; Luobeznova, I.; Goldberg, I.; Gross, Z. *Chem.—Eur. J.* **2003**, *9*, 201.
(9) In this work, we refer to "dioxolene" as a general term for catecholate (Cat), *o*-semiquinonate (SQ), and *o*-benzoquinone (BQ), where Cat, SQ, and BQ are used to distinguish the oxidation state of the ligand.
(10) Bohle, D. S.; Carron, K. T.; Christensen, A. N.; Goodson, P. A.; Powell, A. K. *Organometallics* **1994**, *13*, 1355.

10.1021/ic052180p CCC: $33.50
Published on Web 04/22/2006

been synthesized. Nevertheless, the formal oxidation state of the ligand is maintained for isolated dinuclear complexes in successive redox steps.

However, dioxolene is a noninnocent ligand that shows three forms: catecholate (Cat), *o*-semiquinonate (SQ), and *o*-benzoquinone (BQ). It has been reported that the local energy levels of the dioxolene and transition metal lie close together, and the charge distribution in a dioxolene complex depends on the relative energy levels and the degree of overlap of the dioxolene and metal orbitals.[13,14] In particular, the small relative energy gap between the orbitals of the Ru ion and the orbitals of the dioxolene ligand and the sufficient overlap of these orbitals sometimes lead to an extensive delocalization of the electronic structure.[15,16]

To investigate the advantage of utilizing redox-active ligands in Ru_2 complexes, the $A_2[Ru_2^{6+}(R_4Cat)_4]$ ($A^+ = Li^+$, Na^+, K^+, Rb^+, and *n*-Bu_4N^+; $R_4 = F_4$, Cl_4, Br_4, H_4, 3,5-DTB, and 3,6-DTB; DTB = di-*tert*-butyl) family was synthesized,[17−19] and the oxidation state of the ligands in these complexes was characterized as being the fully reduced catecholate form. In electrochemical studies, the voltammograms of $A_2[Ru_2^{6+}(3,6\text{-DTBCat})_4]$ ($A^+ = Na^+$ (**1a**)[17] and *n*-Bu_4N^+ (**1b**)[18]) showed that a reversible one-electron oxidation readily occurs (potential = −0.74 V vs Fc/Fc^+). The Ru_2 core and dioxolene ligands are redox active, and several types of charge distribution (metal-localized, ligand-localized, and delocalized) can occur in the oxidized species. In this work, we report on the isolation and the crystallographic and spectroscopic characterization of [*n*-Bu_4N]-$[Ru_2(3,6\text{-DTBDiox})_4]$ (**2**).

Experimental Section

Materials and Methods. $[Na(THF)_2]_2[Ru_2(3,6\text{-DTBCat})_4]$ (**1a**·4THF)[17] was synthesized by the literature methods. The other chemicals were purchased from Aldrich Co. (silver tetrafluoroborate ($AgBF_4$) and acetone-d_6) and Tokyo Chemical Industry Co., Ltd. (tetra-*n*-butylammonium bromide (*n*-Bu_4NBr)). All of the solvents (tetrahydrofuran (THF), *n*-hexane (Hex), acetone, and toluene) were distilled by standard methods under a dinitrogen atmosphere. All synthetic operations and measurements were performed under dinitrogen atmosphere by using Schlenk line techniques.

(11) Paw, W.; Keister, J. B.; Lake, C. H.; Churchill, M. R. *Organometallics* **1995**, *14*, 767.
(12) Miyasaka, H.; Chang, H.-C.; Mochizuki, K.; Kitagawa, S. *Inorg. Chem.* **2001**, *40*, 3544.
(13) (a) Pierpont, C. G.; Lange, C. W. *Prog. Inorg. Chem.* **1994**, *41*, 331. (b) Pierpont, C. G. *Coord. Chem. Rev.* **2001**, *219*, 415.
(14) Pierpont, C. G. *Coord. Chem. Rev.* **2001**, *216*, 99.
(15) (a) Haga, M.; Dodsworth, E. S.; Lever, A. B. P. *Inorg. Chem.* **1986**, *25*, 447. (b) Lever, A. B. P.; Auburn, P. R.; Dodsworth, E. S.; Haga, M.; Wei, L.; Melnik, M.; Nevin, W. A. *J. Am. Chem. Soc.* **1988**, *110*, 8076.
(16) (a) Haga, M.; Dodsworth, E. S.; Lever, A. B. P.; Boone, S. R.; Pierpont, C. G. *J. Am. Chem. Soc.* **1986**, *108*, 7413. (b) Boone, S. R.; Pierpont, C. G. *Polyhedron* **1990**, *9*, 2267. (c) Bhattacharya, S.; Boone, S. R.; Fox, G. A.; Pierpont, C. G. *J. Am. Chem. Soc.* **1990**, *112*, 1088. (d) Auburn, P. R.; Dodsworth, E. S.; Haga, M.; Liu, W.; Nevin, W. A.; Lever, A. B. P. *Inorg. Chem.* **1991**, *30*, 3502.
(17) Chang, H.-C.; Mochizuki, K.; Kitagawa, S. *Inorg. Chem.* **2005**, *44*, 3799.
(18) Chang, H.-C.; Mochizuki, K.; Kitagawa, S. *Inorg. Chem.* **2005**, *44*, 3810.
(19) Mochizuki, K.; Chang, H.-C.; Kawamura, T.; Kitagawa, S. *Chem. Lett.* **2005**, *34*, 1662.

Table 1. Crystallographic Data for **1c**·Acetone and **2**·Acetone

	1c·acetone	**2**·acetone
formula	$C_{75}H_{122}NNaO_9Ru_2$	$C_{75}H_{122}NO_9Ru_2$
fw	1406.87	1383.88
cryst syst	monoclinic	tetragonal
space group	*Cc* (No. 9)	$P4_122$ (No. 91)
color of cryst	violet	violet
a, Å	15.740(3)	13.0100(5)
b, Å	21.911(4)	
c, Å	22.556(4)	45.730(2)
β, (deg)	97.912(2)	
V, Å^3	7705(2)	7740.3(5)
T, K	223.2	223.2
Z	4	4
D_{calcd}, g·cm^{-3}	1.213	1.188
μ(Mo Kα), cm^{-1}	4.49	4.41
no. of reflns ($I > 3.0\sigma(I)$)	11 656	7579
no. of params	794	395
GOF	0.94	1.09
R_{int}	0.022	0.024
R^a	0.032	0.032
$R_w{}^b$	0.040	0.043
Flack parameter	0.01(2)	0.00(1)

^{a} $R = \sum||F_o| - |F_c||/\sum|F_o|$. ^{b} $R_w = [\sum w(|F_o| - |F_c|)^2/\sum w|F_o|^2]^{1/2}$.

Synthetic Procedure. [*n*-Bu_4N][{Na(acetone)}{Ru_2(3,6-DTBCat)$_4$}] (1c·Acetone). A THF solution (10 mL) of **1a**·4THF (567 mg, 0.40 mmol) and a THF solution (5 mL) of *n*-Bu_4NBr (129 mg, 0.40 mmol) were combined and stirred for 3 days at room temperature. In this time, a byproduct of this reaction precipitated. The filtrate was dried in vacuo and then recrystallized by layering Hex on the acetone solution of **1c** to obtain single crystals of **1c**·acetone. Yield: 496 mg, 88%. Anal. Calcd for $C_{75}H_{122}NNaO_9Ru_2$ (**1c**·acetone): C, 64.03; H, 8.74; N, 1.00. Found: C, 64.43; H, 8.68; N, 1.02. UV−vis−NIR (λ_{max}/nm (ϵ/M^{-1}·cm^{-1}) in THF): 298 (24 300), 512 (15 100), 650 (sh).

[*n*-Bu_4N][Ru_2(3,6-DTBDiox)$_4$]·acetone (2·Acetone). The compound **2**·acetone can be synthesized by method A or method B.

Method A. A THF solution (5 mL) of **1c**·acetone (281 mg, 0.20 mmol) and a THF solution (30 mL) of $AgBF_4$ (39 mg, 0.20 mmol) were combined and stirred for 1 day. The precipitate of a mixture of Ag metal and $NaBF_4$ was removed by filtration with a mixed solvent (THF/Hex = 1:3). The filtrate was dried in vacuo and then recrystallized by layering Hex on the acetone solution of **2** to obtain single crystals of **2**·acetone.

Method B. A THF solution (5 mL) of **1a**·4THF (709 mg, 0.50 mmol) and a THF solution (30 mL) of $AgBF_4$ (97 mg, 0.50 mmol) were combined and then stirred for 1 day. The precipitate of a mixture of Ag metal and $NaBF_4$ was removed by filtration with a mixed solvent (THF/Hex = 1:3). Drying of the filtrate afforded a violet solid. Cation exchange reaction of this violet solid with *n*-Bu_4NBr (161 mg, 0.50 mmol) was performed in THF by stirring for 3 days, and then precipitates of NaBr were filtered. Recrystallization by layering Hex on the acetone solution of **2** afforded single crystals of **2**·acetone. After extraction with a mixed solvent (THF/Hex = 1:3), the product was purified by repetitive recrystallization under the same condition. Yield: 393 mg, 40%. Anal. Calcd for $C_{75}H_{122}NO_9Ru_2$ (**2**·acetone): C, 65.09; H, 8.89; N, 1.01. Found: C, 65.25; H, 8.91; N, 1.15. UV−vis−NIR (λ_{max}/nm (ϵ/M^{-1}·cm^{-1}) in THF): 303 (25 600), 405 (10 700), 512 (13 200), 650 (sh), 1340 (2100), 2240 (2600).

Crystallographic Data Collection. All crystallographic measurements were performed on a RIGAKU mercury diffractometer with a CCD two-dimensional detector with Mo Kα radiation employing a graphite monochromator ($\lambda = 0.7107$ Å). The sizes of the unit cells were calculated from the reflections collected on

Scheme 1. Synthetic Scheme for Diruthenium Complexes with Ligand-Unsupported Ru−Ru Bonds

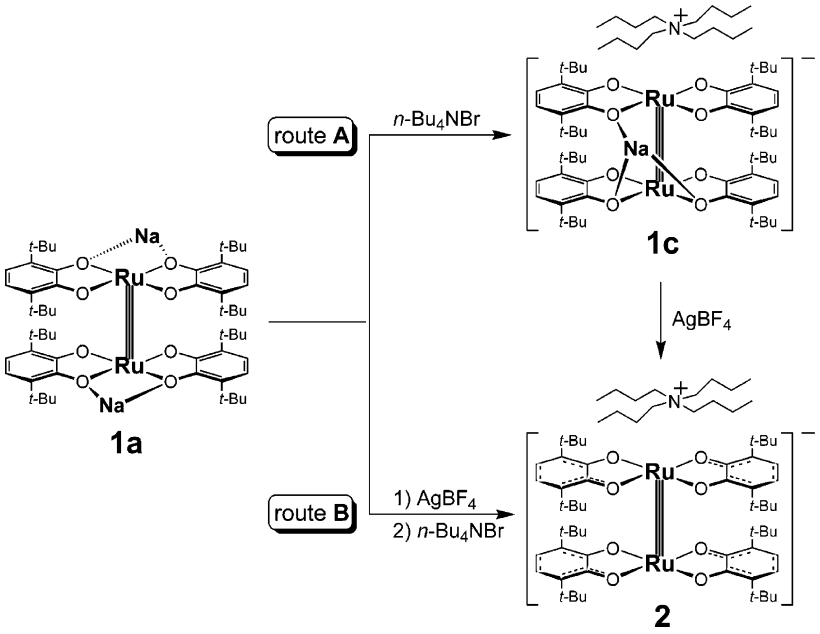

the setting angles of seven frames by changing ω by 15° for each frame. Intensity data were collected in 720 or 2400 frames with ω scan widths of 0.5 or 0.3° under the two or four different ϕ settings for **1c**·acetone or **2**·acetone, respectively. Numerical absorption corrections were performed. All of the crystallographic data are summarized in Table 1. The structures were solved by the Patterson method and expanded using Fourier techniques (PATTY, DIRDIF94).[20] The non-hydrogen atoms were refined anisotropically, whereas the hydrogen atoms were introduced as fixed contributors. The final cycles of the full-matrix least-squares refinements were based on the observed reflections ($I > 3\sigma(I)$). All calculations were performed using the teXsan crystallographic software package of Molecular Structure Corporation.[21] There is a highly disordered *t*-Bu group, C(26)−C(28), in **1c**·acetone.

DFT Calculation. The electronic structure of a model compound, $[Ru_2(H_4Diox)_4]^-$ (**3**), was calculated with the DFT method using the B3LYP functional[22] with the Gaussian 03 program package.[23] For Ru, the LANL2DZ basis set was used together with the effective core potential of Hay and Wadt.[24] For the other elements, the 6-31G[25] basis sets were selected. The contribution of each basis function in each molecular orbital was estimated in the Mulliken population-analysis scheme.[26] The idealized D_2 geometry of model compound **3** was generated by omitting the *t*-Bu substituents from **2** and using the geometry parameters obtained by averaging the crystal-structure data of **2**·acetone.

Physical Measurements. Absorption spectra were recorded on a Hitachi U-3500 spectrophotometer over the range 185−3200 nm at 296 K. EPR spectra at 77 K were recorded with a JEOL JES-RE2X spectrometer operating at X-band. The resonance frequency was measured on an ADVANTEST R5372 microwave frequency counter. The magnetic field sweep was calibrated with the resonance of a JEOL Mn^{2+}/MgO reference sample. For the single-crystal EPR study, the orientation of the crystal was determined after the collections of 637 reflections on a RIGAKU mercury diffractometer with a CCD two-dimensional detector with Mo Kα radiation employing a graphite monochromator. The oriented single crystal was mounted on the quartz stick, embedded in silicon grease, to have it well fixed. The quartz stick with the single crystal was stuck into a quartz tube filled with N_2 gas to protect it from the surrounding atmosphere. EPR spectra were recorded every 15° or 30° over a 150° rotation of the magnetic field in the *bc*- and *ab*-planes. The angles of 0° are defined as the orientations of the magnetic field to the *c*- or *a*-axis for the rotations in the *bc*- and *ab*-planes. The orientation was first estimated visually and then corrected based on the crystallographic symmetrical property for the measurement in the *bc*-plane. This correction to the visual setting was 8.5°. For the measurement in the *ab*-plane, no correction was applied since no appreciable angular dependence was observed.

Results and Discussions

Synthesis and Molecular Structures. Compound **2**, $[n\text{-}Bu_4N][Ru_2(3,6\text{-}DTBDiox)_4]$, was synthesized from **1a** using a two-step reaction process (cation exchange and

(20) Beurskens, P. T.; Admiraal, G.; Beuskens, G.; Bosman, W. P.; de Gelder, R.; Israel, R.; Smits, J. M. M. *The DIRDIF Program System;* Technical Report of the Crystallography Laboratory; University of Nijmegen: The Netherlands, 1994.
(21) *teXsan: Crystal Structure Analysis Package;* Molecular Structure Corporation: The Woodlands, TX, 1992.
(22) (a) Becke, A. D. *J. Chem. Phys.* **1993**, *98*, 5648. (b) Miehlich, B.; Savin, A.; Stoll, H.; Preuss, H. *Chem. Phys. Lett.* **1989**, *157*, 200. (c) Lee, C. T.; Yang, W. T.; Parr, R. G. *Phys. Rev. B* **1988**, *37*, 785.
(23) Frisch, M. J.; Trucks, G. W.; Schlegel, H. B.; Scuseria, G. E.; Robb, M. A.; Cheeseman, J. R.; Montgomery, J. A., Jr.; Vreven, T.; Kudin, K. N.; Burant, J. C.; Millam, J. M.; Iyengar, S. S.; Tomasi, J.; Barone, V.; Mennucci, B.; Cossi, M.; Scalmani, G.; Rega, N.; Petersson, G. A.; Nakatsuji, H.; Hada, M.; Ehara, M.; Toyota, K.; Fukuda, R.; Hasegawa, J.; Ishida, M.; Nakajima, T.; Honda, Y.; Kitao, O.; Nakai, H.; Klene, M.; Li, X.; Knox, J. E.; Hratchian, H. P.; Cross, J. B.; Bakken, V.; Adamo, C.; Jaramillo, J.; Gomperts, R.; Stratmann, R. E.; Yazyev, O.; Austin, A. J.; Cammi, R.; Pomelli, C.; Ochterski, J. W.; Ayala, P. Y.; Morokuma, K.; Voth, G. A.; Salvador, P.; Dannenberg, J. J.; Zakrzewski, V. G.; Dapprich, S.; Daniels, A. D.; Strain, M. C.; Farkas, O.; Malick, D. K.; Rabuck, A. D.; Raghavachari, K.; Foresman, J. B.; Ortiz, J. V.; Cui, Q.; Baboul, A. G.; Clifford, S.; Cioslowski, J.; Stefanov, B. B.; Liu, G.; Liashenko, A.; Piskorz, P.; Komaromi, I.; Martin, R. L.; Fox, D. J.; Keith, T.; Al-Laham, M. A.; Peng, C. Y.; Nanayakkara, A.; Challacombe, M.; Gill, P. M. W.; Johnson, B.; Chen, W.; Wong, M. W.; Gonzalez, C.; Pople, J. A. *Gaussian 03*, revision B.05; Gaussian, Inc.: Wallingford, CT, 2004.
(24) Hay, P. J.; Wadt, W. R. *J. Chem. Phys.* **1985**, *82*, 299.
(25) Hehre, W. J.; Ditchfie, R.; Pople, J. A. *J. Chem. Phys.* **1972**, *56*, 2257.
(26) Mulliken, R. S. *J. Chem. Phys.* **1955**, *23*, 1841.

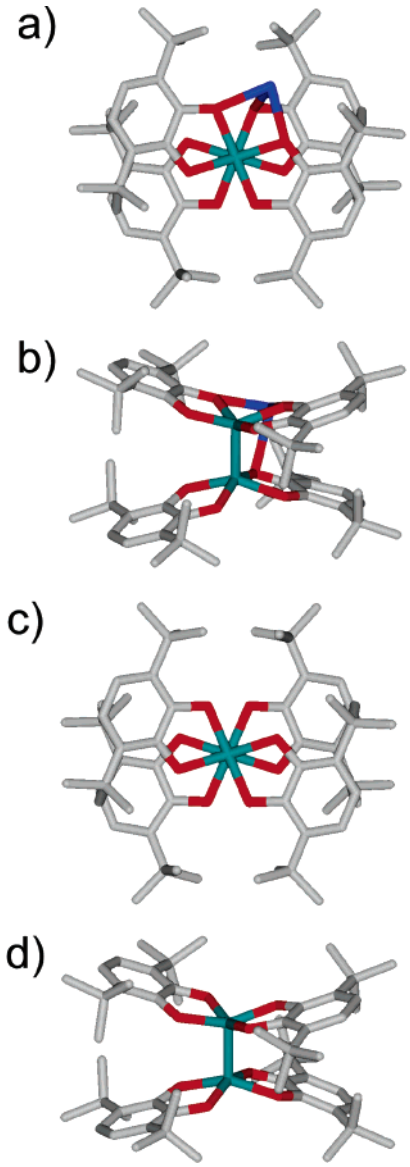

Figure 1. Molecular structures of (a, b) $[Na\{Ru_2(3,6\text{-DTBDiox})_4\}]^-$ anion in **1c**·acetone and (c, d) $[Ru_2(3,6\text{-DTBDiox})_4]^-$ anion in **2**·acetone. Hydrogen atoms are omitted for clarity. The color code is as follows: Ru, green; Na, blue; C, gray; O, red.

one-electron oxidation) according to route A and route B in Scheme 1. Recrystallization by layering Hex onto the acetone solution of **2** afforded single crystals of **2**·acetone. In route A, an intermediate product was isolated as single crystals formulated as $[n\text{-Bu}_4N][\{Na(acetone)\}\{Ru_2(3,6\text{-DTBCat})_4\}]$ (**1c**·acetone).

The molecular structures of **1c**·acetone ($[Na\{Ru_2(3,6\text{-DTBCat})_4\}]^-$) and **2**·acetone ($[Ru_2(3,6\text{-DTBDiox})_4]^-$) are shown in Figure 1, and their structural parameters are summarized in Table 2. The structure of **1c**·acetone is similar to that of **2**·acetone in appearance, except for the coordination of oxygen atoms of the dioxolene ligands to a Na^+ cation (Figure 1). Each Ru atom is coordinated by two 3,6-DTBDiox molecules in a square-planar arrangement, and a direct Ru−Ru bond connects two $[Ru(3,6\text{-DTBDiox})_2]$ units. Both of the Ru atoms in these complexes have no ligands or solvent molecules on the apical position, showing a distorted square-pyramidal coordination geometry. The twist angle along the Ru−Ru bond axis is 51.5° and 49.2° for **1c**·acetone and **2**·acetone, respectively. These values are comparable to those of **1a**·4THF and **1b**·Hex.

Table 2. Representative Structural Parameters for **1a**·4THF, **1b**·Hex, **1c**·Acetone, and **2**·Acetone

	1a·4THF[a]	**1b**·Hex[b]	**1c**·acetone	**2**·acetone
Ru−Ru/Å	2.140(2)	2.1449(7)	2.1538(4)	2.1864(4)
Ru(1)−O(1)/Å	1.99(1)	1.967(3)	1.995(2)	1.957(2)
Ru(1)−O(2)/Å	1.96(2)	1.971(3)	1.948(2)	1.954(2)
Ru(1)−O(3)/Å	1.98(2)	1.971(3)	1.991(3)	1.965(2)
Ru(1)−O(4)/Å	1.94(1)	1.971(3)	1.946(2)	1.966(2)
Ru(1)−O(5)/Å			1.990(2)	
Ru(2)−O(6)/Å			1.958(2)	
Ru(2)−O(7)/Å			1.961(2)	
Ru(2)−O(8)/Å			1.946(2)	
C(1)−O(1)/Å	1.38(3)	1.364(4)	1.380(4)	1.349(3)
C(6)−O(2)/Å	1.40(2)	1.357(5)	1.364(4)	1.347(3)
C(15)−O(3)/Å	1.33(2)	1.352(5)	1.368(4)	1.343(4)
C(20)−O(4)/Å	1.39(3)	1.356(5)	1.356(4)	1.357(5)
C(29)−O(5)/Å			1.376(4)	
C(34)−O(6)/Å			1.361(4)	
C(43)−O(7)/Å			1.370(4)	
C(48)−O(8)/Å			1.369(5)	
deviation, *d*/deg [c]	0.509(5)	0.506(2)	0.495(7), 0.498(7)	0.438(1)
Ru−Ru−O(1)/deg	107.3(5)	106.01(7)	105.42(8)	102.43(6)
Ru−Ru−O(2)/deg	103.8(4)	102.21(8)	103.86(8)	104.79(6)
Ru−Ru−O(3)/deg	103.2(5)	103.54(8)	100.29(7)	103.10(6)
Ru−Ru−O(4)/deg	106.4(3)	107.73(8)	108.82(9)	101.14(6)
Ru−Ru−O(5)/deg			102.88(7)	
Ru−Ru−O(6)/deg			103.91(7)	
Ru−Ru−O(7)/deg			107.46(8)	
Ru−Ru−O(8)/deg			104.49(8)	
twist angle, θ/deg[c]	50.8	48.9	51.5	49.2

[a] Reference 17. [b] Reference 18. [c] See Chart 3 in ref 17.

The averaged structural parameters of $[Ru_2(3,6\text{-DTBCat})_4]^{2-}$ in **1c**·acetone are comparable to those of **1a**·4THF and **1b**·Hex.[17,18] The Ru−Ru bond distance (2.1538(4) Å), average Ru−O bond distance (1.967(2) Å), and average C−O bond distance (1.368(4) Å) in **1c**·acetone are comparable to those of **1a**·4THF and **1b**·Hex. This indicates that the charge distribution of **1c**·acetone is similar to that in **1a**·4THF and **1b**·Hex containing a Ru_2^{6+} core and four 3,6-DTBCat ligands. A comparison of each Ru−O bond distance in **1c**·acetone shows that Ru(1)−O(1), Ru(1)−O(3), and Ru(2)−O(5) bonds are longer than other Ru−O bonds. The crystal structure of **1c**·acetone shows a Na^+ cation located at a site close to the O(1), O(3), and O(5) atoms; therefore, the presence of strong Na−O interactions would serve to lengthen the Ru−O bonds. Similar elongation has been observed in some other dioxolene complexes.[11,27]

On the other hand, **2**·acetone contains only one $n\text{-Bu}_4N^+$ countercation, meaning that the one-electron oxidation of **1c** (or **1a**) successfully proceeded. The diruthenium moiety in **2**·acetone, $[Ru_2(3,6\text{-DTBDiox})_4]^-$, has a cation-free structure that is similar to the structure of $[Ru_2^{6+}(3,6\text{-DTBCat})_4]^{2-}$ in **1b**·Hex, since $n\text{-Bu}_4N^+$ cation has no binding ability. The differences in the structural parameters between **2**·acetone and **1b**·Hex would accurately reflect the effect of one-electron oxidation on the molecular structure. The Ru−Ru bond distance of **2**·acetone, 2.1864(4) Å, is longer by 0.042(1) Å than the Ru−Ru bond distance of **1b**·Hex

(27) Pierpont, C. G. *Inorg. Chem.* **2001**, *40*, 5727.

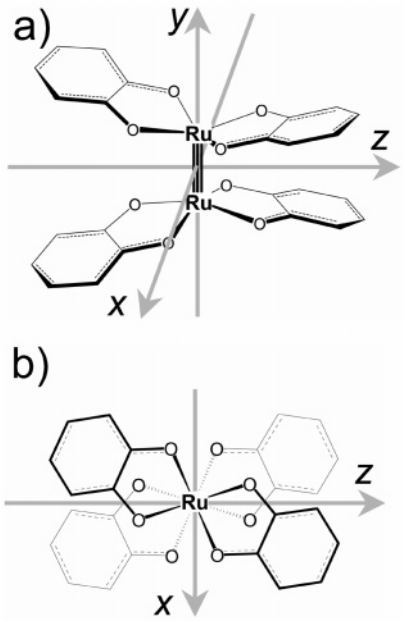

Figure 2. Geometrical model of the $[Ru_2(3,6\text{-DTBDiox})_4]^-$ anion showing the coordinate system used for the **g**-tensors. Hydrogen atoms and *t*-Bu substituents are omitted for clarity.

(2.1449(7) Å). The elongation of the Ru−Ru bond distance decreases the repulsion between the ligands, and thereby the average Ru−Ru−O bond angle in **2**·acetone (102.87(6)°) is smaller than that of **1b**·Hex (104.87(8)°). The average C−O bond distance of **2**·acetone (1.349(4) Å) is comparable to that of **1b**·Hex (1.357(5) Å), but there is a trend that the C−O bond distance of **2**·acetone is slightly shorter than that of **1b**·Hex.

Molecular Packing in the Crystal of 2·Acetone. The $[Ru_2(3,6\text{-DTBDiox})_4]^-$ moiety in **2**·acetone has a pseudo-D_2 geometry and possesses three orthogonal pseudo-2-fold axes. The *y*-axis is defined to be parallel to the Ru−Ru bond, and the *x*- and *z*-axes are defined to the other two pseudo-2-fold axes as shown in Figure 2. The crystal structure of **2**·acetone was determined to be tetragonal with space group $P4_122$. The *a*- and *b*-axes of the unit cell are crystallographically equivalent. Figure 3 shows projections of the molecules in the crystal. Each molecule is classified as either molecule I or molecule II depending on the angle between the molecular axis and the crystallographic axis (Table 3). The *x*-axis in each molecule is parallel to the *a*- or *b*-axis of the unit cell, and the Ru−Ru vector (*y*-axis) is at an angle of approximately 75° to the *c*-axis and is orthogonal to the *b*- or *a*-axis. The adjacent molecules indicated as molecules I and II in Figure 3 are crystallographically equivalent and are related by a 4-fold helical symmetry along the *c*-axis. The *z*-axis of each molecule tilts by an angle of approximately 15° from the *c*-axis.

EPR Study. Axially symmetric EPR spectra of **2** (Figure 4) were observed at 77 K in a toluene frozen solution ($g_{\parallel} = 2.077$ and $g_{\perp} = 1.976$) and pulverized crystals ($g_{\parallel} = 2.073$ and $g_{\perp} = 1.977$) of **2**·acetone (Table 4), although the EPR signal of **2** was too broad to be detected at room temperature in the toluene solution and the solid state. Hyperfine splitting due to $I = {}^5/_2$ ^{99}Ru (12.72% natural abundance) and $I = {}^5/_2$ ^{101}Ru (17.07% natural abundance) or other nuclei was not resolved. The similarity of the **g**-tensors of **2** observed for the frozen solution and for the pulverized crystals shows that even in the crystalline state, the electron spins are practically isolated in the EPR energy- and time-scales. Otherwise, an averaging of the principal *g* values that is characteristic of the mutual arrangement of the diruthenium complexes in the crystal would result in a nonequivalence of the **g**-tensors for the frozen solution and the solid state.

Single-crystal EPR studies will help to determine the relationship between the principal axes of the **g**-tensor and the molecular axes of **2** and help the characterization of its singly occupied molecular orbital (SOMO). The plots shown in Figure 5 show the angular dependence of the *g* value observed during rotation of the magnetic field in the *bc*- and *ab*-planes. A comparison of the angular dependence with the crystal packing diagram (Figure 3) and the EPR spectrum

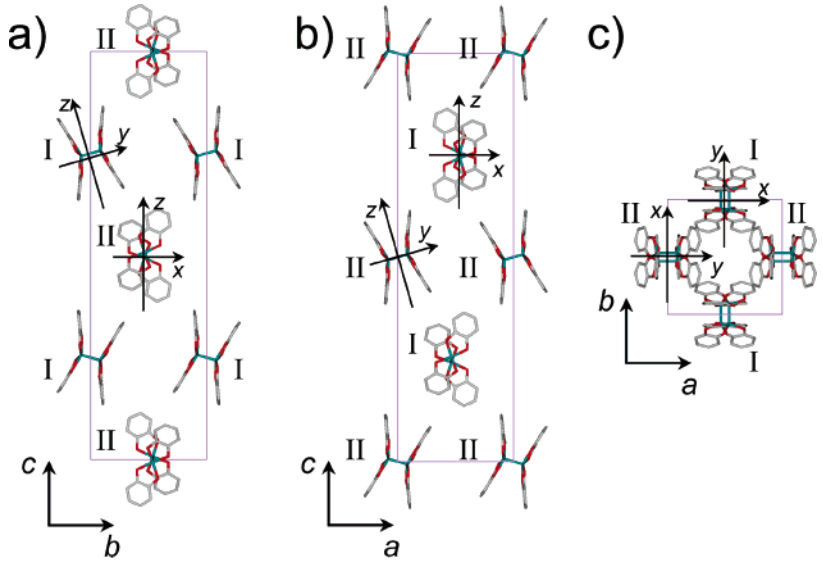

Figure 3. Packing of molecules in crystalline **2**·acetone. Molecule I and molecule II are shown in the figures (I, II). Hydrogen atoms, *t*-Bu substituents, *n*-Bu_4N^+ cation, and interstitial solvent molecules are omitted for clarity.

Table 3. Angles (deg) between Molecular Axes (*x*-, *y*-, and *z*-Axes) and Crystallographic Axes (*a*-, *b*-, and *c*-Axes) of Diruthenium Complexes in Crystalline **2**·Acetone

	x-axis		*y*-axis		*z*-axis	
cryst axis	molecule I	molecule II	molecule I	molecule II	molecule I	molecule II
a-axis	0	90	90	15.6	90	74.4
b-axis	90	0	15.6	90	74.4	90
c-axis	90	90	74.4	74.4	15.6	15.6

Table 4. Principal *g* Values of **2**, Ru_2^{7+} Complexes, and $Na_3[Ru_2^{5+}(R_4Cat)_4]$ (R = F, Cl, Br, and H)

complex	g_1	g_2	g_3	conditions	ref
[*n*-Bu_4N][Ru_2(3,6-DTBDiox)$_4$]	2.077 ($g_{\|\|}$)	1.976 ($g_\perp$)[a]		toluene/77 K	tw[b]
	2.073 ($g_{\|\|}$)	1.977 ($g_\perp$)[a]		pulverized crystal/77 K	tw[b]
$Na_3[Ru_2^{7+}(\mu\text{-OMe})_2(Cl_4Cat)_4]$[c]	2.54	2.01	1.80	powder/77 K	12
$[Ph_4P][Na_2\{Ru_2^{7+}(\mu\text{-OEt})_2(Cl_4Cat)_4\}]$[d]	2.43	2.04	1.86	powder/77 K	12
$[Ru_2^{7+}(dtne)(\mu\text{-O})_2(\mu\text{-}CO_3)][PF_6]$[e]	2.33	2.12	1.97	powder/10 K	28
$Na_3[Ru_2^{5+}(F_4Cat)_4]$	2.13	1.73	1.50	THF/77 K	17
$Na_3[Ru_2^{5+}(Cl_4Cat)_4]$	2.19	1.82	1.53	THF/77 K	17
$Na_3[Ru_2^{5+}(Br_4Cat)_4]$	2.21	1.86	1.56	THF/77 K	17
$Na_3[Ru_2^{5+}(H_4Cat)_4]$	2.01	1.93	1.79	DMF/77 K	17

[a] The principal values, g_x and g_z, are accidentally equivalent (see text). [b] tw = this work. [c] $Na_3[Ru_2^{7+}(\mu\text{-OMe})_2(Cl_4Cat)_4]$ = [Na(benzo-15-crown-5)$_2$][{$(Na(MeOH)_3\}_2\{Ru_2(Cl_4Cat)_4(\mu\text{-OMe})_2\}$]. [d] $[Ph_4P][Na_2\{Ru_2^{7+}(\mu\text{-OEt})_2(Cl_4Cat)_4\}]$ = $[Ph_4P][\{Na(EtOH)_3\}_2\{Ru_2^{7+}(Cl_4Cat)_4(\mu\text{-OEt})_2\}]$. [e] dtne = 1,2-bis(1,4,7-triazacyclononan-1-yl)ethane.

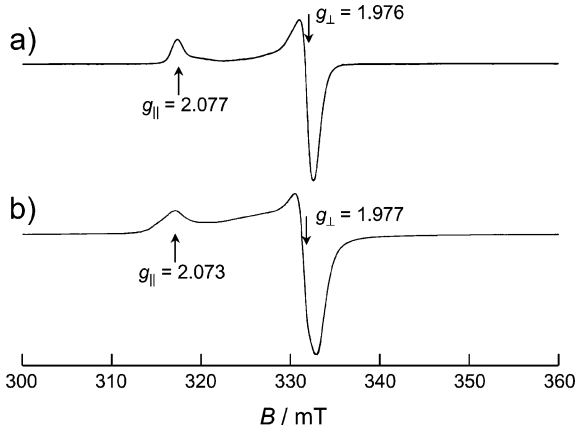

Figure 4. X-band EPR spectra at 77 K: (a) frozen toluene solution of **2** and (b) pulverized crystals of **2**·acetone.

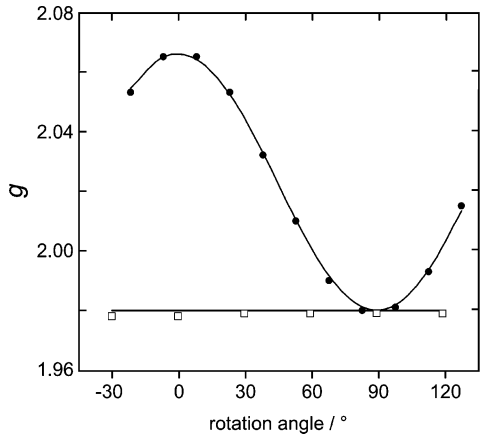

Figure 5. Angular dependence of the single-crystal EPR spectra of **2**·acetone at 77 K. The rotations of field direction in the *bc*-plane (●) and in the *ab*-plane (□) are shown. The solid lines are angular dependence of the *g* values calculated with the principal *g* values for pulverized crystals.

of pulverized crystals (Figure 4) leads to the assignment of the $g_{||}$-axis as the molecular *z*-axis (Figure 2) and the $g_\perp$-axes as the molecular *x*- and *y*-axes (Figure 2). Thus, the principal *g* values related to the molecular axes are: $g_{xx} = g_{yy} = g_\perp = 1.977$, and $g_{zz} = g_{||} = 2.073$ in crystalline **2**·acetone at 77 K. The solid lines shown in Figure 5 show the *g* values calculated based on these assignments. The angular dependence of the calculated *g* values agrees satisfactorily with the observed angular dependence, supporting the current assignment of the principal *g*-axes.

Table 5. Relative Energy Levels of the Low-Lying Doublet States of **3**

		spin population (%) and character of SOMO			
electronic state	relative energy (kJ/mol)	metal		ligands	
^2A	63.35	~0		~100	π_L
$^2B_1$	0	18.2	twisted π_{RuRu}	81.8	π_L
$^2B_2$	83.98	~0		~100	π_L
$^2B_3$	51.45	7.8	twisted π_{RuRu}	92.2	π_L

DFT Calculation. DFT calculations were performed on a model structure of **3** with a D_2 geometry. This dinuclear structure was modeled based on the average values of the structural parameters of **2**·acetone. The electronic ground state of this diruthenium structure was found to be $^2B_1$. Energies of low-lying excited states (^2A, $^2B_2$, and $^2B_3$) were calculated for the same geometry and listed in Table 5. The SOMO of the $^2B_1$ state shown in Figure 6 indicates an extensive mixing of the diruthenium d_π orbitals with the

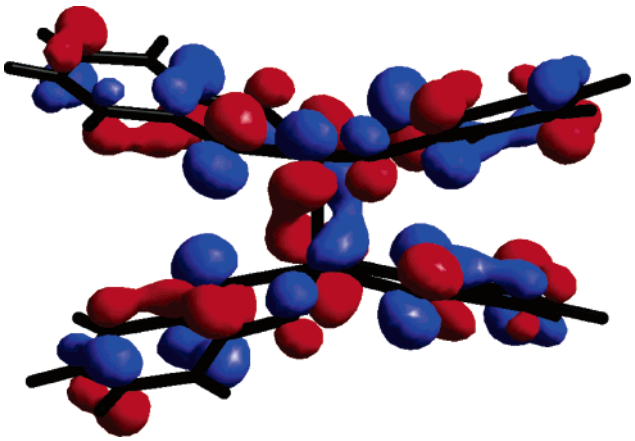

Figure 6. Shape of the SOMO of **3**.

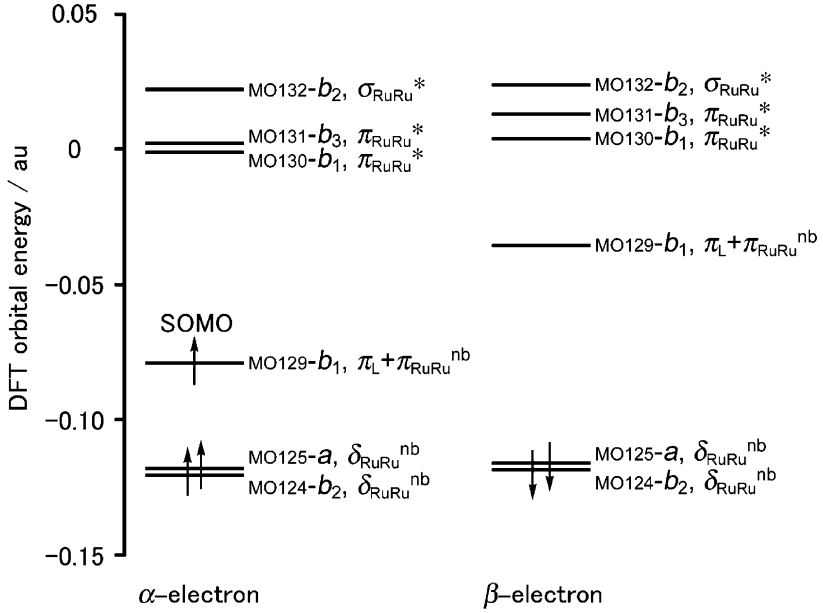

Figure 7. Energy level diagram for **3**. SOMO and other MOs with significant Ru_2 core components are drawn in the figure.

dioxolene frontier π orbitals. The spin population was estimated to be approximately 18% and 82% for the Ru_2 core and the ligands, respectively. Figure 7 shows the energy level diagram of the SOMO and high-lying doubly occupied and low-lying unoccupied MOs having a considerable contribution of the Ru_2-core components. This diagram should be considered in the analysis of the **g**-tensor in the following section.

Formal Oxidation States of Diruthenium Core and Dioxolene in $[Ru_2(3,6\text{-DTBDiox})_4]^-$. The starting materials, **1a** or **1c**, possess $[Ru_2^{6+}(3,6\text{-DTBCat})]^{2-}$ dinuclear moieties, making three models conceivable for the electronic structure of **2**. The first model is $[Ru_2^{7+}(3,6\text{-DTBCat})_4]^-$ formed by the metal-centered oxidation, the second model is $[Ru_2^{6+}(3,6\text{-DTBCat})_3(3,6\text{-DTBSQ})]^-$ formed by the ligand-based oxidation, and the third model is $[Ru_2(3,6\text{-DTBDiox})_4]^-$ with a delocalized electronic structure, the resonance hybrid (i.e., mixture) of the first and the second models.

As mentioned above, the appreciable shifts in principal values of the **g**-tensor of **2** from the free-electron value ($g_e = 2.002$) lead to the conclusion that the SOMO has a Ru_2 core component. The observed shifts are smaller than those of Ru_2^{5+} complexes having similar molecular structures[17] and Ru_2^{7+} complexes[12,28] possessing ruthenium-centered SOMOs (Table 4). However, they are obviously larger than the shifts of g values of the mononuclear dioxolene complexes of Ru possessing SQ-centered SOMOs ($\Delta g \approx 0.00$).[29] Thus, the unpaired electron in **2** is suggested to be delocalized over the Ru_2 core and dioxolene ligands, as discussed for the EPR spectra of some mononuclear compounds.[15] Therefore, the most probable SOMO for **2** is a linear combination of the π HOMOs of the Cat ligands and the Ru−Ru π-type orbital. We note that the latter orbital is the only Ru_2 orbital that is symmetry-allowed to extensively mix with the catecholate π MOs.

The SOMO of **3** is calculated as the MO129-b_1, which is formed by the extensive mixing of the Ru−Ru π-type orbital and the π HOMOs of the Cat ligands. This is consistent with the "medium-range" shifts of the principal g values of **2** from g_e. The shape of the SOMO in Figure 6 indicates that it has the π antibonding character of the C−O bonds. This is consistent with the trend that the C−O bond distance decreases with oxidation.

Further qualitative analysis of the shift in **g**-tensor is required to examine the SOMO of the current species based on the DFT results calculated for the model complex **3**. The shifts in principal g values from g_e are induced by the spin−orbit coupling of the unpaired electron.[30] In the simple molecular orbital theory scheme, the shift in the principal g value from g_e is given by[30]

$$\Delta g_{zz} = g_{zz} - g_e = 2\sum_{\lambda}^{\neq p} \langle \Phi_p | \sum_k l_k^z | \Phi_\lambda \rangle \langle \Phi_\lambda | \sum_k \zeta_k l_k^z | \Phi_p \rangle (\epsilon_p - \epsilon_\lambda)^{-1} \quad (1)$$

where ϕ and ϵ are the MO and its orbital energy, respectively, with the subscripts p and λ denoting the unpaired-electron orbital and another orbital, respectively. The term ζ_k denotes one-electron spin−orbit coupling constant for the kth atomic orbital, and the integration of the z-component of the orbital angular momentum around the nucleus of the kth atomic orbital, l_k^z, is to be performed only for the one-center type. The valence-shell orbital spin−orbit coupling in **2** is much larger for the Ru 4d atomic orbital (878 cm^{-1})[31] than for the atomic orbitals of the other elements (the second largest spin−orbit coupling constant in **2** is 151 cm^{-1} for the oxygen 2p orbital).[32] This difference in ζ values shows that, for

(28) Geilenkirchen, A.; Neubold, P.; Schneider, R.; Wieghardt, K.; Florke, U.; Haupt, H. J.; Nuber, B. *J. Chem. Soc., Dalton Trans.* **1994**, 457.
(29) Sugimoto, H.; Tanaka, K. *J. Organomet. Chem.* **2001**, *622*, 280.
(30) (a) Stone, A. J. *Proc. R. Soc. London* **1963**, *A271*, 424. (b) Stone, A. J. *Mol. Phys.* **1963**, *6*, 509.
(31) Goodman, B. A.; Raynor, J. B. *Adv. Inorg. Chem. Radiochem.* **1970**, *13*, 135.
(32) Carrington, A.; McLachlan, A. D. *Introduction to Magnetic Resonance;* Harper & Row: New York, 1967.

qualitative analysis of the **g**-tensor, we can focus on the Ru 4d component of the SOMO and the other molecular orbitals and neglect all the other components of this equation calculating the shift in **g**-tensor.

We qualitatively estimated the shifts in principal *g* values based on our DFT results for **3** (Figures 6 and 7) and compared the data with the observed shifts in *g* values of **2**. Since l^x, l^y, and l^z in D_2 symmetry belong to b_3, b_2, and b_1, respectively, then the shifts in principal *g* values Δg_{xx}, Δg_{yy}, and Δg_{zz} for **3** having a ground state of $^2B_1$ are induced by the mixing of the doubly occupied or unoccupied b_2, b_3, and a orbitals, respectively, into the b_1 SOMO by the spin−orbit coupling term in eq 1. Since the numerators in eq 1 are positive, then the high-lying doubly occupied MOs with a large Ru character induce a positive shift in *g* values and low-lying unoccupied MOs induce a negative shift in *g* values. A straightforward estimation of Δg_{xx} is difficult, because Figure 7 shows that the MOs with the b_2 symmetry appear in the low-lying unoccupied level (MO132-b_2,σ_{RuRu}*) and the high-lying doubly occupied level (MO124-b_2,δ_{RuRu}^{nb}) giving mutually opposing contributions to the Δg_{xx}. The doubly occupied MO125-a,δ_{RuRu}^{nb} orbital induces a positive shift in g_{zz}, and the unoccupied MO131-b_3,π_{RuRu}* orbital induces a negative shift in g_{yy}. This quantitative analysis is consistent with the observed shifts in *g* values for **2** and supports our current assignment of the SOMO of **2**.

As shown in Figure 8, electronic absorption spectrum of **2** with a $[Ru_2(3,6\text{-DTBDiox})_4]^-$ moiety shows two characteristic broad bands in the near-IR region, whereas **1b** with a $[Ru_2(3,6\text{-DTBCat})_4]^{2-}$ moiety has no absorption bands in this region. The band at 2240 nm could be assigned to anintervalence charge-transfer band of Cat → SQ,[14,33] indicating the ligands in **2** have SQ character, and the other band at 1340 nm is presumably attributable to the charge transfer of Ru_2 → SQ.

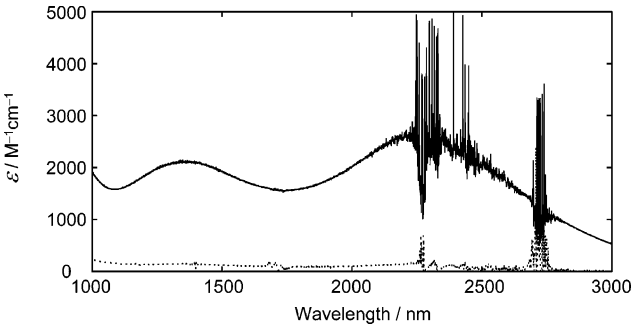

Figure 8. Near-IR spectra of **1b** (···) and **2** (—). Spikes in the 2400 and 2700 nm regions are due to the unbalanced cancellation of solvent absorptions.

Concluding Remarks

The one-electron oxidation of **1a** or **1c** with a $[Ru_2^{6+}(3,6\text{-DTBCat})_4]^{2-}$ moiety affords **2** possessing a $[Ru_2(3,6\text{-DTBDiox})_4]^-$ moiety, and the SOMO of **2** is best explained by the extensive mixing of the diruthenium d_π orbitals with the dioxolene frontier π orbitals. This is an example of a Ru_2 complex where the utilization of redox-active ligands into a dinuclear complex expanded the degree of freedom in the electronic structure.

Acknowledgment. This work was supported by a Grant-In-Aid for Science Research from the Ministry of Education, Culture, Sports, Science and Technology, Japan.

Supporting Information Available: X-ray crystallographic data of **1c**·acetone and **2**·acetone in CIF format. This material is available free of charge via the Internet at http://pubs.acs.org.

IC052180P

(33) (a) Chang, H. C.; Miyasaka, H.; Kitagawa, S. *Inorg. Chem.* **2001**, *40*, 146. (b) Wada, T.; Fujihara, T.; Tomori, M.; Ooyama, D.; Tanaka, K. *Bull. Chem. Soc. Jpn.* **2004**, *77*, 741.